ELSEVIER

Chemical Engineering Journal 131 (2007) 73–82

Chemical Engineering Journal

www.elsevier.com/locate/cej

Topochemical approach of kinetics of the reduction of hematite to wüstite

K. Piotrowski [a], K. Mondal [b], T. Wiltowski [b,c,*], P. Dydo [d], G. Rizeg [e]

[a] *Department of Chemical & Process Engineering, Silesian University of Technology, M. Strzody 7, 44-101 Gliwice, Poland*
[b] *Department of Mechanical Engineering & Energy Processes, Southern Illinois University Carbondale, Carbondale, IL 62901, USA*
[c] *Coal Research Center, Southern Illinois University Carbondale, Carbondale, IL 62901, USA*
[d] *Department of Inorganic Chemistry & Technology, Silesian University of Technology, Krzywoustego 6, 44-101 Gliwice, Poland*
[e] *General Electric-Energy & Environmental Research Corporation, Irvine, CA 92618, USA*

Received 5 January 2006; received in revised form 8 December 2006; accepted 18 December 2006

Abstract

The kinetics of hematite (Fe_2O_3) to wüstite (FeO) reduction has been investigated. Kinetic parameters have been estimated based on the thermogravimetric data. The Avrami–Erofe'ev equation of coupled nucleation and growth processes was successfully applied to describe the initial stages of the process, while four diffusion equations were tested to model the final stages of the process. It was found that the initial stage can be interpreted theoretically as the crystals' nucleation and 1D growth at the gas/iron oxide(s) interface, which gradually shifts to diffusion control. Kinetic and diffusion regions for various temperatures (within the 700–900 °C range) were identified. The value of activation energy ΔE_a of the reaction was estimated and compared with the literature data.

Keywords: TGA data; Topochemical reaction; Iron-oxide(s) reduction; Isothermal gas–solid reaction kinetics; Avrami–Erofe'ev model; Hematite; Magnetite; Wüstite

1. Introduction

The reduction of hematite (Fe_2O_3) to wüstite (FeO) during the oxidation of CO, present in the syngas, to CO_2 is an important industrial reaction that may potentially lead to a pure hydrogen gas stream. This is a complex gas–solid, redox-type reaction in which the kinetics is closely related to the structural changes in the intermediate iron oxide (magnetite) that is formed during the reaction time. Additionally, in the advanced stages of the process, the progress of reduction is strongly controlled by internal diffusion of the reducing gas. The pore structure, determined by hematite–magnetite and magnetite–wüstite lattice transformations, can considerably affect the overall process rate. In addition, the surface carbon deposition (Boudouard reaction) can affect the diffusion resistances [1–48].

Many researchers have tried to develop a universal kinetic equation for gaseous reduction of iron oxides. However, it was only possible to obtain a set of independent equations, useful for the description of the reduction process within a certain range of reaction conditions [1,15,16,21,22]. Some authors have evaluated the reduction mechanism in great depth, improving the theoretical models on which the rate equations are applied [6,7,12,16,18–20]. It was generally concluded that the consecutive reduction of iron oxides by means of a mixture of gaseous agents is an example of a complex heterogeneous gas–solid reaction(s), which effective rate is significantly affected by both intrinsic topochemical kinetics on one hand and – equally important – diffusional mass transfer effects on the other.

The mechanisms of these reactions have been reviewed in detail by Turkdogan et al. [18–20]. They reported that although there is a general agreement on the chemical nature of the individual rate-controlling reactions, the behavior of the overall process kinetics, especially due to the complex transformations and synergistic interrelations between all the factors, is still not well understood. Thus, there has been considerable disagreement and diversity in the reaction rate constant values that are reported in the literature. The disruptive stresses set-up during the transformation of Fe_2O_3 to Fe_3O_4 result in noticeable structural changes occurring during the reaction [12].

The TGA analysis of the reduction of hematite in a pure CO stream within the 800–900 °C range was previously presented by Avrami [49]. A kinetic model was proposed, approaching

* Corresponding author at: Coal Research Center, Southern Illinois University Carbondale, Carbondale, IL 62901, USA. Tel.: +1 618 453 7000.
E-mail address: tomek@siu.edu (T. Wiltowski).

1385-8947/$ – see front matter © 2007 Elsevier B.V. All rights reserved.
doi:10.1016/j.cej.2006.12.024

Nomenclature

A	constant in the Arrhenius equation, Eqs. (5) and (6) (K)
ΔE_a	activation energy (kJ/mol)
k	kinetic constant (min^{-1})
k_0	kinetic constant in the Arrhenius equation, Eqs. (5) and (6) (min^{-1})
m	sample mass (g)
n	constant associated with the geometry of the system
R	statistical correlation coefficient
t	process time (min)
T	process temperature (°C)

Greek symbols

α	fraction reacted till time t (thus, conversion degree for the time t)
β	constant, partially depended both on nucleation frequency and rate of grain growth
δ	contribution of the nucleation process in the overall kinetics (Eq. (4))
λ	dimensionality of crystal growth (Eq. (4))

Subscripts

AE	Avrami–Erofe'ev model
d	diffusion model
0	initial state
10%	corresponded to 10%-decrease in the initial weight

this complex system by pseudo-first-order irreversible rate kinetics, considering the consecutive reduction of iron oxides: $Fe_2O_3 \rightarrow Fe_3O_4 \rightarrow FeO \rightarrow Fe$, the Boudouard reaction and iron carbide (Fe_3C) formation. Since many industrial direct reduction processes use gas feeds derived from reforming hydrocarbons, containing both CO and H_2, the reported experiments were performed using a reducing mixture composed of both CO and H_2. Additionally, considering the practical aspect of cyclic regeneration within the $Fe_2O_3 \leftrightarrow FeO$ system, the reaction's course was limited only to the hematite–wüstite range. A topochemical approach was employed to evaluate the theoretical mechanisms of reactions and their kinetics.

2. Experimental procedure and results

The kinetics of the hematite–magnetite–wüstite reduction process was determined by monitoring the change of the specimen's weight during its transformation under selected isothermal conditions. The experiments were performed using a *Perkin-Elmer TGA-7* thermogravimetric analyzer with a *TAC 7/DX* control unit driven by *Pyris* software (sample's weight measurement performed every 0.25 s).

Fe_2O_3 powder (*PEA Ridge Iron Ore Co.*, 91 μm average size determined by the particle size analyzer *Microtrac S3500*, average density 2.18 g/cm^3 and specific surface area 10.63 m^2/g determined by liquid nitrogen BET analyzer measurements) was initially preheated (10 °C/min) under flowing nitrogen to the predetermined temperature (selected from the 700–900 °C range) and then isothermally processed under a reducing atmosphere (gas mixture composition: 90% N_2 + 5.7% CO + 4.3% H_2). The volumetric flow rate of the reducing mixture was 30 mL/min. Its composition was strictly controlled by blending the pure gases in the required proportions. Before entering the thermogravimetric reactor, gases were dried using the molecular sieve moisture trap *Hydro-Purge II, Alltech*. About 12 mg of a fresh Fe_2O_3 sample was used in each experiment.

Considering the following iron oxide(s) reduction sequence:

$$Fe_2O_3 \rightarrow Fe_3O_4 \rightarrow FeO$$

and taking into account that Fe_3O_4 can be considered as an intermediate state between Fe_2O_3 and FeO (thus reported as solid mixture Fe_2O_3·FeO), the theoretical weight change of iron oxide was calculated according to the stoichiometry of the following parallel reactions:

$$Fe_2O_3 + CO \rightarrow 2FeO + CO_2$$

$$Fe_2O_3 + H_2 \rightarrow 2FeO + H_2O$$

It can be noted that, based on the above reactions' stoichiometry, the complete reduction of Fe_2O_3 to FeO corresponds to a 10% decrease of the initial sample weight. On the other hand, a complete reduction of Fe_2O_3 to metallic Fe results in a 30% decrease in the initial weight of the sample.

The experimental data (decrease in sample's weight, m) were then recalculated to obtain a conversion degree, α (of Fe_2O_3 to FeO) as a function of time, t, using the following formula:

$$\alpha(t) = \frac{m_0 - m(t)}{m_0 - m_{10\%}} \quad (1)$$

To improve the clarity of graphical presentation, the raw experimental data (actual sample's weight) were recalculated and presented in a more convenient, uniform coordinate system, where "1" corresponds to initial mass of Fe_2O_3 sample, while "0" corresponds to a 30% mass decrease state (Fe).

The $m_{10\%}$ (actually as a line corresponded to value of 0.666 of a sample's relative mass – thus FeO state) parameter was directly superimposed graphically onto the reduction data (Fig. 1a and b, various time ranges). A distinctly visible plateau is observed at 700 °C. This may indicate the decrease in the $Fe_2O_3 \rightarrow FeO$ reaction rate before the further reduction to metallic iron will occur. However, at 810 and 900 °C that "$m_{10\%}$ line" serves only as "marker" to identify the theoretical moments of final transformation of Fe_2O_3 into FeO.

The $\alpha = f(t)$ experimental profiles, calculated with Eq. (1) and corresponded to different process temperatures, are presented in Fig. 2.

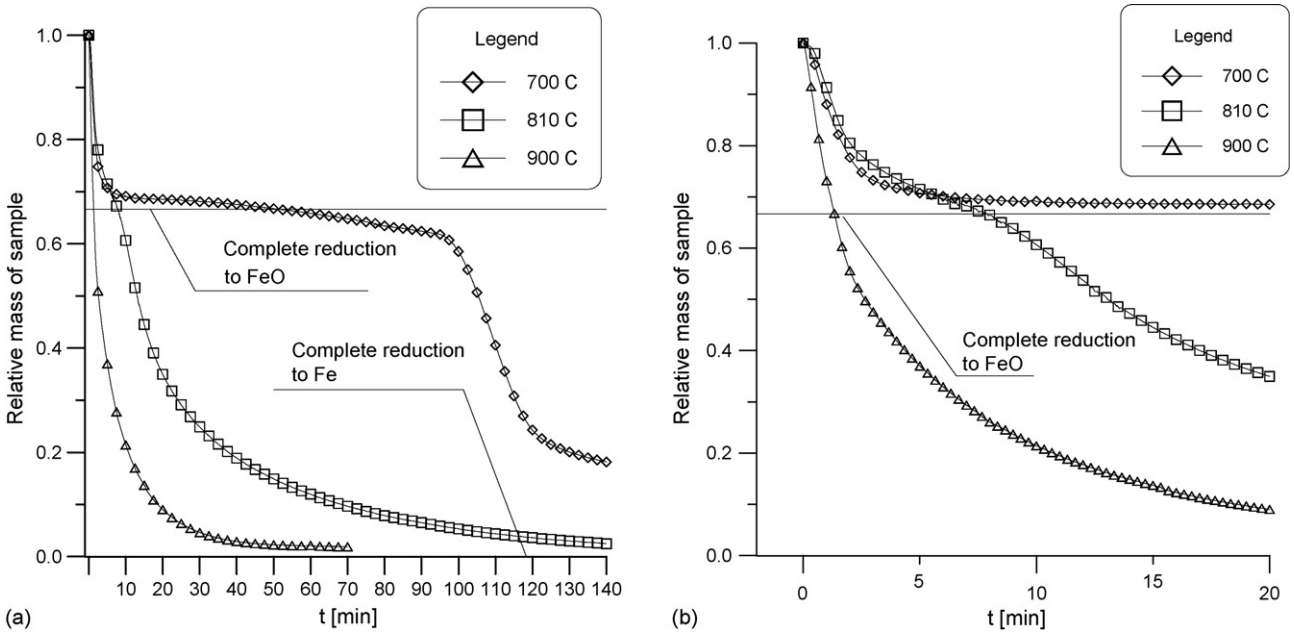

Fig. 1. (a) TGA experimental data for the selected temperature values studied (full range 0–150 min)—indication of the weight-loss limits corresponding to FeO (10% value of 2/3 on the graph) and Fe (30% value of 0 on the graph). (b) TGA experimental data for the selected temperature values studied (limited range 0–30 min)—indication of the weight-loss limits corresponding to FeO (10% value of 2/3 on the graph) and Fe (30% value of 0 on the graph).

3. Kinetic models of topochemical reactions

All $\alpha = f(t)$ isotherm plots (Fig. 2) are sigmoid-shaped and exhibit three distinct regions: incubation, acceleration, and decay. It is observed, that, with an increase in process temperature, the transformed solids exhibit a shorter incubation period (in Fig. 2 it is clearly visible especially at temperatures above 850 °C) and reduce at a more rapid rate.

The $\alpha(t)$ data sets were then analyzed according to the Hancock and Sharp's method of comparing the kinetics of isothermal solid-state reactions [49–57]. This method is based on the general equation describing nucleation and growth processes:

$$\alpha = 1 - \exp(-\beta t^n) \tag{2}$$

$$\ln(-\ln(1-\alpha)) = \ln\beta + n\ln t \tag{3}$$

where α is the Fe_2O_3 fraction reacted till certain time, t (thus, Fe_2O_3 to FeO conversion degree corresponding to the time t, as mentioned in Eq. (1)); β the constant, partially depended both on nucleation frequency and the grain growth rate (thus indirectly on process temperature); n is the exponent associated with the system geometry.

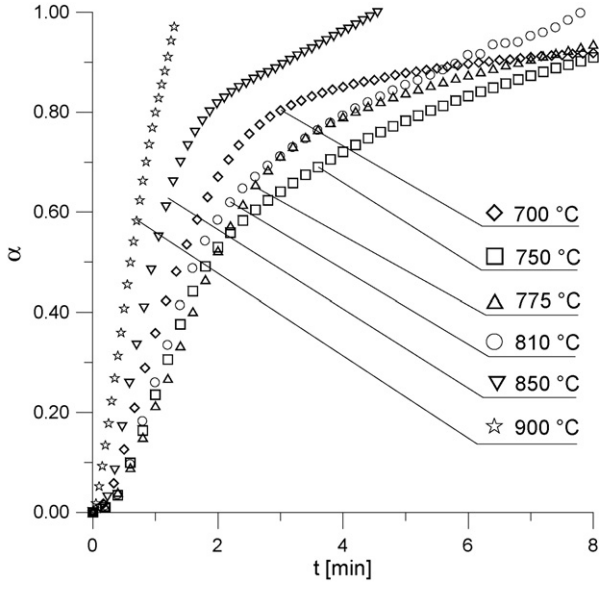

Fig. 2. Conversion degree vs. time for the selected process temperatures studied.

This sigmoid shape of $\alpha(t)$ (see Fig. 2) is commonly observed for some certain kind of topochemical solid-state reactions and is typically analyzed by applying the kinetic model proposed by Avrami and Erofe'ev [49–52]. This model assumes that "germ nuclei" of the new phase are distributed randomly within the solid. Following a nucleation event, the grains grow throughout the old phase until the transformation is completed. The sigmoid shape of kinetic plots may be analyzed by dividing each curve into three regions corresponding theoretically to: induction period ($0 < \alpha < 0.15$), acceleratory region ($0.15 < \alpha < 0.50$) and a deceleratory region ($0.50 < \alpha < 1$) [53]. The induction period is dominated mainly by nucleation while the acceleratory one tends to be dominated by growth phenomena. The deceleratory region corresponds to the termination of growth upon impingement of different growth regions or at the grain boundaries [53]. Values of the slope (n) of recalculated plots (see Eq. (3)) within the $0.15 < \alpha < 0.50$ range indicates multiple reaction pathways and the most probable mechanisms [53]. The plots of the experimental data, recalculated by applying Eq. (3), are presented in Fig. 3 and their statistical analysis is presented in Table 1.

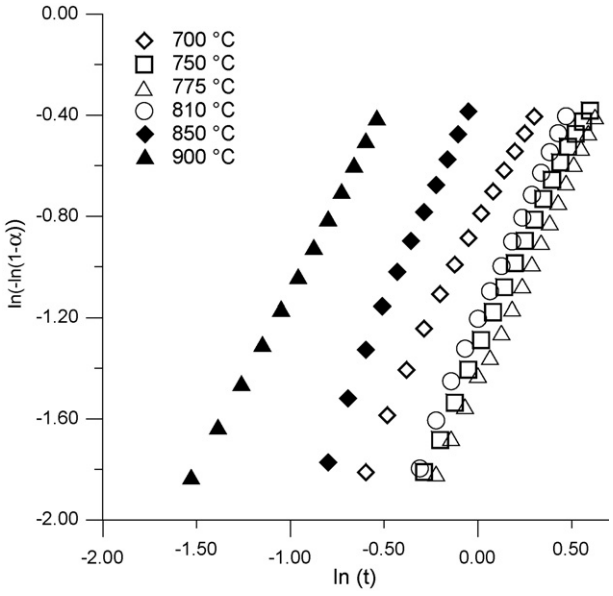

Fig. 3. Plots of the Eq. (3)—illustration of Hancock and Sharp's procedure (for the selected T values).

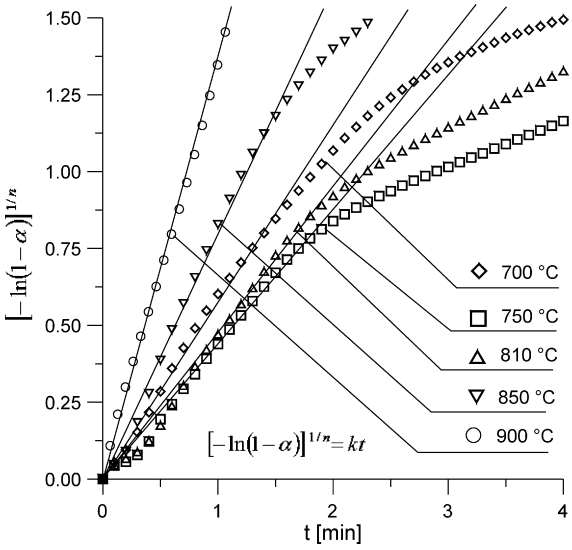

Fig. 4. Graphical presentation of Eq. (4) courses for the selected process temperature values studied.

An average value of $n = 1.63$ was obtained. This value, as well as the sigmoidal shape of the $\alpha = f(t)$ plots, suggest that the Avrami–Erofe'ev universal kinetic model, Eq. (4), may be applicable for the $Fe_2O_3 \rightarrow FeO$ reduction reaction (thus phase transition) modeling:

$$[-\ln(1-\alpha)]^{1/n} = kt \tag{4}$$

Eq. (4) is recognized as the generalized kinetic equation of solid-state chemical reactions. It has been derived independently by Johnson and Mehl [55], Avrami [49–51] and Erofe'ev [52]. Its special case for $n = 1$ represents (pseudo) first-order kinetics. The parameter n, appearing in the exponent of Eq. (4), is equivalent to the slope (n) resulting from the Sharp–Hancock's plot (see Eq. (3), Fig. 3). In this equation, describing nucleation and crystal growth on a phase-boundary surface, the slope n is interpreted as the sum of $\lambda + \delta$, where λ is the dimensionality of growth (an integer value: 1, 2 or 3); δ is the contribution of the nucleation process to the overall kinetics (it varies between 0 and 1, where 0 corresponds to instantaneous nucleation, and 1 to a very slow nucleation rate) [53].

The values of $n = 1$–2 are observed for 1D growth, $n = 2$–3 for 2D growth, and $n = 3$–4 for 3D growth [53]. Thus, the experimental data can be fitted to the Avrami–Erofe'ev equation assuming an average value of $n = 1.6$ (Table 1) to evaluate the kinetic constant (k) values for each process temperature used. From a theoretical point of view, it indicates that this phase transition proceeds through 1D growth process (since $\lambda = 1$) with a moderate contribution of nucleation (as $\delta = 0.6$). Additionally, considering the intermediate (non-integer) value of the n parameter, it can be concluded that these topochemical changes may be controlled, at least partially, by heat transfer phenomena within the reaction microenvironment [55]. Plots of Eq. (4) for selected temperatures are presented in Fig. 4 (the plot for $T = 775$ °C was omitted here only for the effect of the clarity of presentation).

Table 1
Parameters of Eq. (3) for the temperatures studied—Hancock and Sharp's method applied

Exp. no.	T (°C)	n	$\ln \beta$	No. of data	R
1	700	1.51	−0.83178	52	0.996
2	750	1.65	−1.32264	67	0.998
3	775	1.66	−1.45234	68	0.999
4	810	1.74	−1.21435	56	0.999
5	850	1.78	−0.27657	32	0.997
6	900	1.43	0.34746	24	0.999

Presentation of the data recalculated as $[-\ln(1-\alpha)]^{1/n}$ versus reaction time, t (for assumed value of $n = 1.6$) for each temperature shows directly the corresponded "time ranges" in which the process follows the theoretically proposed mechanism (thus producing linear segments). The data within those time ranges (thus presenting linear trends) were used to evaluate the corresponded reaction rate constant k values (see Table 2).

The Avrami–Erofe'ev model's (Eq. (4)) predictions begin to deviate essentially from the experimental data within the deceleratory region ($0.50 < \alpha < 1$), with the largest deviations observed for the lowest temperature values tested (700 and 750 °C). The process becomes diffusion-controlled then and the actual mechanism of this following reaction's stage differs from the one that controlled it initially. The diffusion layer on the surface prevents α from reaching unity relatively quickly. Consequently, the $\alpha = f(t)$ data within the $0.50 < \alpha < 1$ range must thus be modeled theoretically with the use of several diffusion mechanisms. Each of these mechanism have to be valid individually within the defined, shifted reaction time (see Table 2).

Graphical comparison between the experimental and modeled values of $\alpha = f(t)$ using a combined approach that integrates two physical–chemical phenomena of different natures: the Avrami–Erofe'ev topochemical kinetic model ($n = 1.6$) with the simplest, 1D diffusion kinetic model (parabolic diffusion model) in their validity ranges is presented in Fig. 5a and b.

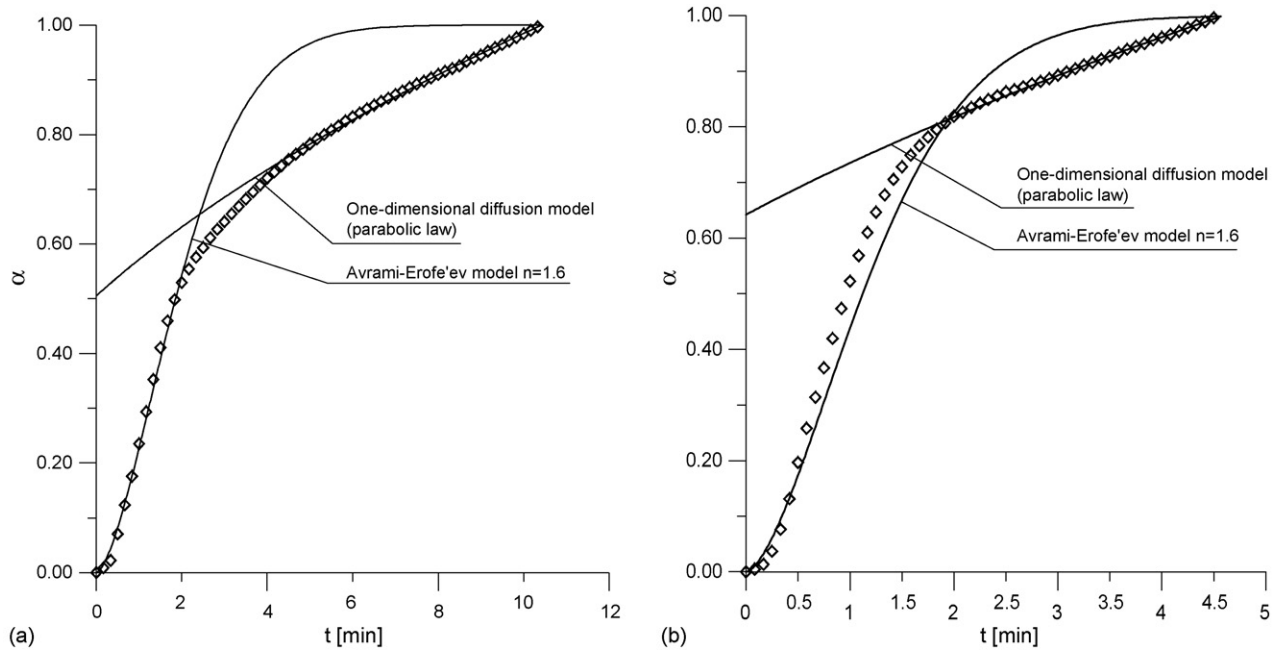

Fig. 5. (a) Comparison of experimental TGA data (◊) (T = 775 °C) with the two kinetic models applied in this study: Avrami–Erofe'ev phase change model (n = 1.6, k_{AE} = 0.3920, R = 0.998) and 1D diffusion model (parabolic law) (k_d = 0.0549, R = 0.999) (Table 2). (b) Comparison of experimental TGA data (◊) (T = 850 °C) with the two kinetic models applied in this study: Avrami–Erofe'ev phase change model (n = 1.6, k_{AE} = 0.7094, R = 0.990) and 1D diffusion model (parabolic law) (k_d = 0.1280, R = 0.999) (Table 2).

It is clearly visible, that the first stage of the process is governed by topochemical reaction as its course is strictly compatible with the appropriate Avrami–Erofe'ev model. Theoretical predictions of topochemical model are highly overestimated as it is seen in Fig. 5a and b because focusing only on surface processes of iron oxide(s) this model does not take into account real physical phenomena—mass transfer resistances through more or less (additionally gradually increasing) layers of a reaction product. In case of (theoretical) no mass transfer resistances the overall process kinetics could be approached using an Avrami–Erofe'ev model solely. However, in real processes – even in laboratory TGA scale experiments – some resistances appear, causing more and more visible deviating of real data from the model predictions, till the process from the kinetic point of view becomes totally diffusion-controlled, what is practically confirmed by strict compatibility with, e.g. the 1D diffusion model (parabolic law).

The data from Table 2 (concerning intrinsic Avrami–Erofe'ev kinetics) were then applied to obtain the activation energy values from the Arrhenius equation. The $\ln(k) = f(1/T)$ plot (Eqs. (5) and (6)) is a straight-line with a negative slope (see Fig. 6):

$$k = k_0 \exp\left(-\frac{A}{T}\right) = k_0 \exp\left(-\frac{\Delta E_a}{8.314T}\right) \quad (5)$$

$$\ln k = \ln k_0 - A\frac{1}{T} \quad (6)$$

From the regression calculations, the following were obtained: A = 6992 K and $\ln k_0$ = 5.737. Thus, ΔE_a = 58.131 kJ/mol (13.9 kcal/mol) and k_0 = 310 min^{-1} (R = 0.914).

It should be noted, however, that only the (8.4–9.5) × 10^{-4} range of the 1/T parameter was taken into consideration (Fig. 6) for the regression calculations because of (discussed further in the next section) physical peculiarities associated with the reaction rate perturbations at lower values of temperature (vicinities of 750 °C [1,18,21,22]). Taking into account the occurrence of this extreme in the $\ln(k)$ parameter values within the specified temperature range, only the data corresponding to T = 775–900 °C range were taken under further consideration for the above described calculation.

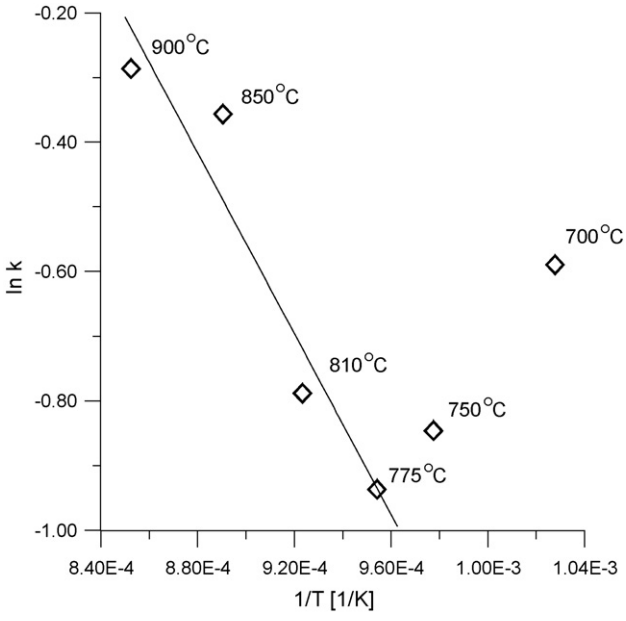

Fig. 6. Arrhenius plot $\ln k = f(1/T)$—evaluation of activation energy of the process.

Table 2
The kinetic models applied: their parameter values, validity ranges and statistically (linear regression) accuracy

Model	Process temperature (isothermal reduction conditions)					
	700 °C	750 °C	775 °C	810 °C	850 °C	900 °C
Kinetic process controlling						
Avrami–Erofe'ev phase-change model [53], $[-\ln(1-\alpha)]^{1/n} = kt$	0–2.5 min; $\alpha < 0.75$; $k_{AE} = 0.5546$; $R = 0.998$	0–2 min; $\alpha < 0.55$; $k_{AE} = 0.4292$; $R = 0.998$	0–3 min; $\alpha < 0.75$; $k_{AE} = 0.3920$; $R = 0.998$	0–2.5 min; $\alpha < 0.65$; $k_{AE} = 0.4546$; $R = 0.997$	0–2 min; $\alpha < 0.80$; $k_{AE} = 0.7094$; $R = 0.990$	0–1.3 min; $\alpha = 0$–1; $k_{AE} = 0.7509$; $R = 0.999$
Diffusion process controlling						
1D diffusion [62], $\alpha^2 = kt$	1–2.5 min; $k_d = 0.3086$; $R = 0.997$	4–11 min; $k_d = 0.0714$; $R = 0.997$	5–11 min; $k_d = 0.0549$; $R = 0.999$	2.5–5.5 min; $k_d = 0.1120$; $R = 0.994$	3–4.5 min; $k_d = 0.1280$; $R = 0.999$	0.6–1.3 min; $k_d = 0.9909$; $R = 0.999$
2D diffusion [62], $(1-\alpha)\ln(1-\alpha) + \alpha = kt$	1–2.5 min; $k_d = 0.2366$; $R = 0.999$	3–9 min; $k_d = 0.0829$; $R = 0.999$	4–10 min; $k_d = 0.0764$; $R = 0.997$	2.5–5.5 min; $k_d = 0.1102$; $R = 0.999$	Non-linear in the whole range	Non-linear in the whole range
3D diffusion (Jander) [64], $[1-\sqrt[3]{1-\alpha}]^2 = kt$	Non-linear in the whole range	2–8 min; $k_d = 0.0413$; $R = 0.995$	4–7 min; $k_d = 0.0433$; $R = 0.999$	2.5–5.5 min; $k_d = 0.0546$; $R = 0.998$	Non-linear in the whole range	Non-linear in the whole range
Diffusion model of Ginstling and Brounshtein, Seth and Ross [62,63], $(1-(2\alpha/3)) - (1-\alpha)^{2/3} = kt$	Non-linear in the whole range	2–8 min; $k_d = 0.0246$; $R = 0.999$	5–8 min; $k_d = 0.0233$; $R = 0.999$	2.5–5.5 min; $k_d = 0.0322$; $R = 0.999$	Non-linear in the whole range	Non-linear in the whole range

4. Discussion

TGA curves of $Fe_2O_3 \rightarrow FeO$ reduction within the investigated $T = 700$–$900\,^{\circ}C$ range and presented as $\alpha = f(t)$, sigmoidal in nature, grow steeper with increasing temperature (Fig. 2). This suggests that the required process time for the total conversion of Fe_2O_3 to FeO shortens considerably with increasing temperature.

Nucleation and growth mechanisms developed by the Avrami–Erofe'ev model can be successfully applied to describe this heterogeneous reaction, which is closely coupled with the phase transformations. In such reactions, a new phase is nucleated by germ nuclei contained in the old phase followed by growth. The Avrami–Erofe'ev equation is applicable to a wide range of mechanisms except the final step that is usually diffusion-controlled [53]. Therefore, this equation was used for modeling the overall reaction pathways occurring in the initial process stage.

The average value of $n = 1.63$ can also be interpreted theoretically using the Hancock and Sharp's tabulation [54]. From this point of view it can be treated as an intermediate model among several other "pure" topochemical cases, such as the phase-boundary-controlled reaction for cylinder ($n = 1.11$) or sphere ($n = 1.07$), zero-order reaction ($n = 1.24$) and the strictly 2D Avrami–Erofe'ev reaction (phase transformations, nucleation and crystals growth) ($n = 2$). This interpretation is in agreement with the published data of other researchers (e.g. [23,44,58–61]). Shimokawabe [58] proposed a random nucleation model for the hematite reduction while Sastri et al. [59] applied the phase-boundary mechanism. Tiernan et al. [23] observed the occurrence of both mechanisms: $Fe_2O_3 \rightarrow Fe_3O_4$ reaction obeyed the phase-boundary model while the $Fe_3O_4 \rightarrow Fe$ obeyed the random nucleation model. El-Geassy [60], on the basis of high-temperature (900–1200 °C) Fe_2O_3 reduction data, concluded that the $Fe_2O_3 \rightarrow FeO$ reaction was governed by a mixed reaction mechanism in the early stages followed by interfacial chemical reaction, while the $FeO \rightarrow Fe$ was governed by a mixed chemical reaction. Similar observations were reported by Moon et al. [45] and Moon and Rhee [61]. However, it cannot be excluded that the mixed mechanism frequently observed may result from simultaneous recrystallization in one or more of the iron oxide phases present within the system under study. On the other hand, in such complex systems more than one of the possible theoretical chemical and physical phenomena may be governing simultaneously. Any particular dominant phenomenon may change as the reaction proceeds. It can be concluded, that for practical reasons the mass transfer should also be considered in a detailed kinetic analysis of the entire process. For example, the reaction rate constant values, presented in Table 2 (representing the intrinsic rates of reaction), do not necessarily indicate the maximum rates that can be achieved in practice, since they will be strongly depended on the limitations imposed by mass transfer (e.g. subsequent diffusion effects). However, these kinetic parameters have been evaluated on the basis of the data representing the initial stage of the process thus not considerably affected by diffusional resistances. For this reason they may indicate the theoretical upper limit of any reduction rate

achievable in these systems (for the given process conditions). Fundamentally, such kinetic data are very useful, for example as a base for accurate and reliable determination of the activation energy values. However, in the light of presented observations the heat transfer effects in the reaction microenvironment resulting from the enthalpy of reaction should also be incorporated in the detailed physical models.

At higher conversions, the experimental α values are lower than those predicted by Eq. (4). Although this may be affected by the uncertainty in the experimental conditions or by the sample's particle size distribution and/or other geometrical factors, these deviations are mainly attributed to the formation of a layer of solid product encapsulating the reactant. As the thickness of this porous layer of the lower iron oxides grows, the subsequent diffusional process begins to play an essential role and becomes the rate-controlling mechanism. Thus, the diffusional kinetic models should then be applied (Table 2).

The termination of growth upon impingement of different regions or at grain boundaries results in the formation of the deceleratory region [53]. In this region, considerable deviation between Avrami's single crystal model and the data from powder samples is often observed, due to variations in crystallite and/or grain size [53]. Similarly, the induction period contributes to the small deviations from linearity, visible especially at the beginning of the process (within the lowest α range in Figs. 4, 5a and b) for the lowest values of temperature.

The surface area of the sample changes during the process course because of external and internal cracking, indirectly affecting the local heat transfer conditions in the microenvironment of the reaction, where small deviations from homogeneity in the assumed isothermal conditions may also occur considering the endothermic nature of the $Fe_2O_3 \rightarrow FeO$ reaction that causes some local, unwanted effects, e.g. self-cooling of the sample. Shrinkage that occured during the reduction of hematite to magnetite and magnetite to wüstite (different crystallographic structures) can cause some local tension in solid structures [24]. However, the Avrami–Erofe'ev type of "contracting volume equation" theoretically incorporates all these effects, taking into consideration overlapping volumes during the reaction course.

All the graphs (Figs. 4, 5a and b) indicate qualitatively (e.g. linear sections for appropriate time ranges as it is in Fig. 4, or coincidence with experimental data presented in Fig. 5a and b) the accuracy of the assumed kinetic models of complex topochemical reactions in their validity regions (Table 2).

Analyzing the data in Table 2 and presented in Figs. 2, 4 and 6 it can be seen that the reduction rate is remarkably delayed within the vicinity of 750 °C. This peculiarity in the temperature dependency was often observed in the temperature range of 650–750 °C and in the vicinity of 920 °C, as well. It was reported and explained in literature [1,19] in terms of the obstruction of intraparticle diffusion on account of blockage of pores due to the fusion the Fe_3O_4 particles. In these "rate minima temperature ranges" sintering of fresh, spontaneously formed metallic iron (or iron carbide) around wüstite grains can isolate them from direct contact with the reducing gas, considerably decreasing the observed reduction rate [21,22]. In the complex topochemical transformations described above, these side-reactions (appearance of Fe and Fe_3C) are unavoidable, even under precise process control.

Table 3 provides the results of other experiments reported in the accessible literature, especially the mechanism and the activation energies of the Fe_2O_3 reduction process and compares the published results with those reported in this study. It should

Table 3
Summary of activation energy values reported in literature and comparison with the own result

Source	Reduction step	Reduction mechanism	ΔE_a (kJ/mol)	Experimental method
Current investigation	$Fe_2O_3 \rightarrow FeO$	Phase boundary	58.13	Isothermal TGA
Shimokawabe [58]	$Fe_2O_3 \rightarrow Fe_3O_4$	Random nucleation	33.27–74	Linear heating rate
Sastri et al. [59]	$Fe_2O_3 \rightarrow Fe$	Phase boundary	57–73	Isothermal TGA
Tiernan et al. [23]	$Fe_2O_3 \rightarrow Fe_3O_4$	Not determined	106	Linear heating rate
Tiernan et al. [23]	$Fe_2O_3 \rightarrow Fe_3O_4$	Phase boundary	96	CRTA "*rate-jump*"
Trushenski et al. [24]	$Fe_2O_3 \rightarrow Fe_3O_4$	Non-topochemical approach, complex model	69–100	Isothermal TGA
	$Fe_3O_4 \rightarrow FeO$		64.46–78.27	Isothermal TGA
	$FeO \rightarrow Fe$		115.94	Isothermal TGA
El-Geassy et al. [21,22]	$Fe_2O_3 \rightarrow Fe$	Phase boundary limited by gaseous diffusion	31.6–53.57	Isothermal, 200 μm size
	(Fe_3O_4, FeO, Fe_3C, C present)		9.54–21.51	Isothermal, 100 μm size
Nasr et al. [12]	$Fe_2O_3 \rightarrow Fe$ (FeO, Fe_3C, Fe_2C, C present)	Initial stage, combination of gaseous diffusion and interfacial chemical reaction	28.92	Isothermal TGA
		Final stage, $T < 900$ °C, gaseous diffusion	23.81	Isothermal TGA
		Final stage, $T > 1000$ °C, gaseous diffusion	14.98	Isothermal TGA
Moon et al. [45]	$Fe_2O_3 \rightarrow FeO$ (H_2); $Fe_2O_3 \rightarrow FeO$ (CO)	Chemical surface reaction, intraparticle diffusion through the reduced layer	19.84–42.15	Isothermal TGA

be noted that the values of the activation energy reported here are comparable with those cited in the literature.

The variations in the activation energy values reported by different authors (Table 3) are probably due to the differences in the experimental conditions, such as average particle size and partial pressure of the reducing gases, which are known to exert considerable effect on the overall process and its kinetics. For example, El-Geassy et al. [21,22] studied the effect of particle size on the iron oxide reduction. In their studies, the activation energies were found to increase with particle size. For 100 μm Fe_2O_3 particles, activation energies in the range of 9.5–21.5 kJ mol^{-1} were obtained for various experimental conditions. It should be noted here, that their chemical models involved the complete reduction of iron oxide to a metallic iron in a single step. Sastri et al. [59] reported that freshly formed Fe particles in the presence of low levels of water vapor (2–7.5% in the reducing mixture) have an autocatalytic effect on the reduction process. They reported activation energies (Fe_2O_3 reduction to Fe) in the range of 57–73 kJ mol^{-1}. Studies conducted by Shimokawabe [58] showed, that for temperatures below 700 °C the reduction of Fe_2O_3 proceeded via a distinct two step mechanism (Fe_2O_3 to Fe_3O_4 and Fe_3O_4 to Fe) while in reduction experiments conducted at temperatures beyond 900 °C both steps occurred simultaneously. Activation energy values reported by these authors ranged from 33.27 to 74 kJ mol^{-1}. The differences in the activation energies reported in literature can also be attributed to the method of Fe_2O_3 synthesis. For example, Shimokawabe [58] prepared α-Fe_2O_3 by decomposing iron salts in air (in 500–1200 °C). He found that the samples prepared at higher decomposition temperatures showed higher activation energies compared to those prepared at lower temperatures, presumably due to the lower reactivity of the relatively larger particles formed during the high-temperature decomposition process. Sastri et al. [59] observed that the pretreatment of the iron oxide at 850 °C resulted in increase of activation energy to 73 kJ mol^{-1} in comparison to the activation energy value of 57 kJ mol^{-1} for the untreated sample.

Analyzing the kinetic data within the diffusion-controlled region (Table 2) it can be concluded that the simplest, one-dimensional model (1D, parabolic diffusion model) can be successfully applied to describe time-profiles of all the data-sets (isotherms) without any significant loss in statistical accuracy (R = 0.994–0.999) in contrast to alternate, more complex models of diffusion.

For T = 700 °C, two diffusion models 1D and 2D diffusion, producing linear segments of appropriate modified equations can be applied. It has to be pointed out, that both the Avrami–Erofe'ev model and these two diffusion models are valid within the same initial time period (0–2.5 min) indicating existence of the mixed control mechanism at this temperature (both surface reaction/phase change and diffusion).

When reaction temperature is increased to 750 °C, the deviation between those mechanisms begins to be more distinct. Namely, the Avrami–Erofe'ev equation is valid within the 0–2 min time period, since diffusion plays an important role within the following 2–11 min time period. An interesting observation can be made, however, within the limits of experimental and statistical error. With the increase of reaction time, there is a slow "shift" between the "strict" diffusion mechanisms—from the 3D model (corresponding to 2–8 min), via 2D model (3–9 min) to 1D model (corresponding to 4–11 min). This can be attributed to the transient conditions during the formation of a more and more thicker layer of product(s) on the initial surface of substrate, gradually developing more stable conditions for a diffusion process directed to the largest concentration gradient (driving force oriented), namely vertically oriented to the phase-boundary surface. Both 3D models, developed for spherical particles, are valid within the same time period (2–8 min). Statistically, the fourth model developed by Ginstling and Brounshtein, and Seth and Ross [62,63] was found to fit the data best with an R value of 0.999.

Similar observations were made when the reaction was conducted at 775 °C. Under these conditions, the "shift" from the 4–7 min range (corresponded to 3D diffusion model) to the 5–11 min range (corresponded to 1D diffusion model) is visible. The last two diffusion models are valid within the 4–8 min period with the same correlation accuracy, R = 0.999. The surface-controlled kinetic model (Avrami–Erofe'ev model) is valid within the 0–3 min, and is distinctly separated from the later pronounced diffusion effects.

For entire temperature range being studied, a general observation can be made. The time range corresponding to the Avrami–Erofe'ev model's validity gradually shrinks—from 0–3 min (775 °C) to 0–1.3 min (900 °C). This is closely coupled with the increase in the reaction rate with the temperature increment (considering the endothermic nature of the reducing process), resulting in the faster formation of intermediate and final product layer covering the initial surface of hematite.

When the temperature increases to 810 °C, it is observed that the "intermediate" region disappears. Thus, diffusion equations (2.5–5.5 min) are valid immediately after the Avrami–Erofe'ev model's validity ends (0–2.5 min). The differences between the diffusion models quality can be practically neglected since the all the R values are within the 0.994–0.999 limits and possible small deviations between their accuracies can be primarily attributed to the experimental error and/or regression procedure accuracy.

In the highest temperature range (850–900 °C) only the 1D diffusion model is valid, with high statistical accuracy (R = 0.999), while other diffusion models show highly non-linear courses which can be interpreted as a proof of their non-validity. This observation can be explained theoretically by the relatively quick formation of the diffusional layer, thus directing the diffusion stream according to the concentration gradient without any initial transient perturbations associated with relatively slow structural changes within the intermediate iron oxides as it is observed within the lower temperature range.

5. Conclusions

Iron oxide is an ideal candidate as an oxygen transfer compound for the oxidation of carbon monoxide to carbon dioxide in the processes used in the production of high purity

hydrogen from syngas for two reasons. First, it provides high oxidation rates for CO. The produced CO_2 can be, in turn, relatively easily removed from the gaseous stream by a number of commercially available absorption/adsorption/chemisorption technologies. This results in the production of a high purity hydrogen stream. The second advantage is that the enthalpy of the Fe_2O_3–FeO transition is ideal for the water-gas shift reaction to occur. In addition, Fe_2O_3 is known to behave as a catalyst for the water-gas shift reaction. However, the reduction of iron oxide is not a simple process and depends on both surface reaction and phase transformation. Obtaining a complete understanding of the individual reactions will considerably help in the design of a better process for pure hydrogen production and in predicting the results obtained from such a process. A topochemical approach provides deeper insights into the mechanisms of such gas–solid reactions. The following are the major findings obtained in this study:

- The sigmoidal nature of $\alpha = f(t)$ suggests the initial occurrence of a phase-change-controlled reaction mechanism, commonly described by the general (thus flexible) Avrami–Erofe'ev topochemical kinetic model with the acceptable statistical accuracy ($R = 0.990$–0.999).
- The Avrami–Erofe'ev equation (1D crystal growth with moderate-rate nucleation, assumed exponent $n = 1.6$) integrated with the selected diffusion mechanism (e.g. the simplest in mathematical form, parabolic 1D diffusion equation) adequately models the time-course of the $Fe_2O_3 \rightarrow FeO$ reduction process over the entire (0–1) conversion range for all isotherms within the investigated $T = 700$–$900\,^{\circ}C$ range.
- The activation energy value evaluated (58.13 kJ/mol) is within the range of results presented in the literature (9.54–115.94 kJ/mol) and acquired for considerably diversified experimental conditions.

Acknowledgements

Funding for this research was provided by US Department of Energy under contract DE-FC26-00FT40974. The authors also acknowledge GE-EER for their support.

References

[1] M. Tokuda, H. Yoshikoshi, M. Ohtani, Trans. ISIJ 13 (1973) 350.
[2] R.A.D. Rodriguez, A.N. Conejo, E.B. Bedolla, Proceedings of the Ironmaking Conference, 2002, p. 493.
[3] G. Bian, A. Oonuki, N. Koizumi, H. Nomoto, M. Yamada, J. Mol. Catal. A: Chem. 186 (1–2) (2002) 203.
[4] D.B. Bukur, M. Koranne, X. Lang, K.R.P.M. Rao, G.P. Huffman, Appl. Catal. A: Gen. 126 (1) (1995) 85.
[5] T. Suzuki, K. Saeki, Y. Mayama, T. Hirai, S. Hayashi, React. Kinet. Catal. Lett. 44 (2) (1991) 489.
[6] S.K. El-Rahaiby, Y.K. Rao, Metal. Trans. B 10 (1979) 257.
[7] P.C. Hayes, Metal. Trans. B 10 (1979) 211.
[8] K. Yagita, Y. Iguchi, S. Hayashi, J. Iron Steel Inst. Jpn. 89 (10) (2003) 1005.
[9] Sharan, N. Chakraborti, Zeit. Metall. 81 (2) (1990) 91.
[10] N. Towhidi, Steel Res. 74 (10) (2003) 595.
[11] Y. Iguchi, K. Matsubara, S. Hayashi, Proceedings of the 2nd International Conference on Proc. Mater. Prop., 2000, p. 541.
[12] M.I. Nasr, A.A. Omar, M.M. Hessien, A.A. El-Geassy, ISIJ Int. 36 (2) (1996) 164.
[13] L.P. Nikanorova, V.M. Antonova, Khim. Tverd. Topl. 25 (4) (1991) 138.
[14] K. Sin-Myoung, J. Sanghoon, M. Dong-Joon, L. Il-Ock, ISIJ Int. 36 (2) (1996) 156.
[15] R.D. Doherty, K.M. Hutchings, J.D. Smith, S. Yörük, Metal. Trans. B 16 (1985) 425.
[16] J. Bessieres, A. Bessieres, J.J. Heizmann, Int. J. Hydrogen Energy 5 (1980) 585.
[17] G.M. Mehrotra, R.H. Tupkary, Ind. J. Technol. 12 (1974) 322.
[18] E.T. Turkdogan, J.V. Vinters, Metal. Trans. 2 (1971) 3175.
[19] E.T. Turkdogan, R.G. Olsson, J.V. Vinters, Metal. Trans. 2 (1971) 3189.
[20] E.T. Turkdogan, J.V. Vinters, Metal. Trans. 3 (1972) 1561.
[21] A.A. El-Geassy, K.A. Shehata, S.Y. Ezz, Trans. ISIJ 17 (1977) 629.
[22] A.A. El-Geassy, M.I. Nasr, M.M. Hessien, ISIJ Int. 36 (6) (1996) 640.
[23] M.J. Tiernan, P.A. Barnes, G.M.B. Parkes, J. Phys. Chem. B 105 (2001) 220.
[24] S.P. Trushenski, K. Li, W.O. Philbrook, Metal. Trans. 5 (1974) 1149.
[25] R.H. Prasad, Tupkary, Ind. J. Technol. 11 (1973) 245.
[26] X. Shuang, Acta Polit. Scand., Chem. Technol. Metal. Ser. 217 (1994) 1.
[27] M.A. Hastaoglu, I.A. Abba, Metal. Mater. Trans. B: Process Metal. Mater. Process Sci. 29 (1) (1998) 229.
[28] H. Ono-Nakazato, T. Yonezawa, T. Usui, ISIJ Int. 43 (10) (2003) 1502.
[29] M.I. Nasr, A.A. Omar, M.H. Khedr, A.A. El-Geassy, ISIJ Int. 35 (9) (1995) 1043.
[30] V. Hacker, R. Fankhauser, G. Faleschini, H. Fuchs, K. Friedrich, M. Muhr, K. Kordesch, J. Power Sources 86 (1–2) (2000) 531.
[31] H. Ono-Nakazato, Y. Tsubone, T. Usui, ISIJ Int. 42 (5) (2002) 482.
[32] N.K. Nath, N. Chakraborti, R. Shekhar, Scand. J. Metal. 24 (3) (1995) 121.
[33] E.D. Negri, O.M. Alfano, M.G. Chiovetta, Ind. Eng. Chem. Res. 30 (3) (1991) 474.
[34] Zhou, K. Suzuki, V. Sahajwalla, J.M. Cadogan, Scand. J. Metal. 28 (2) (1999) 65.
[35] S. Hayashi, O. Asai, S. Sawai, Y. Iguchi, J. Iron Steel Inst. Jpn. 85 (3) (1999) 208.
[36] G. Munteanu, P. Budrugeac, L. Ilieva, T. Tabakova, D. Andreeva, E. Segal, J. Mater. Sci. 38 (9) (2003) 1995.
[37] S. Hayashi, Y. Iguchi, J. Iron Steel Inst. Jpn. 86 (10) (2000) 641.
[38] R. Sime, J. Kuehni, L. D'Souza, E. Elizondo, S. Biollaz, Int. J. Hydrogen Energy 28 (5) (2003) 491.
[39] H.W. Kang, W.S. Chung, T. Murayama, Y. Ono, ISIJ Int. 38 (11) (1998) 1194.
[40] A.K. Ray, K.K. Prasad, P.K. Sen, Sol. State Ionics 50 (3–4) (1992) 217.
[41] A.A. El-Geassy, ISIJ Int. 37 (9) (1997) 844.
[42] H.W. Kang, W.S. Chung, T. Murayama, Y. Ono, ISIJ Int. 38 (4) (1998) 324.
[43] H. Randall, R. Doepper, A. Renken, Ind. Eng. Chem. Res. 36 (8) (1997) 2996.
[44] Y. Iguchi, J. Iron Steel Inst. Jpn. 85 (6) (1999) 447.
[45] I.J. Moon, C.H. Rhee, D.J. Min, Steel Res. 69 (8) (1998) 302.
[46] E.H. Ahra, A. Modaressi, J. Bessieres, J.J. Heizmann, Sol. State Ionics 81 (1–2) (1995) 5.
[47] Steinfeld, A. Frei, P. Kuhn, Metal. Mater. Trans. B: Process Metal. Mater. Process Sci. 26 (3) (1995) 509.
[48] K. Mondal, H. Lorethova, E. Hippo, T. Wiltowski, S.B. Lalvani, Fuel Process Technol. 86 (2004) 33.
[49] M. Avrami, J. Chem. Phys. 7 (1939) 1103.
[50] M. Avrami, J. Chem. Phys. 8 (1940) 212.
[51] M. Avrami, J. Chem. Phys. 9 (1941) 177.
[52] B.V.C.R. Erofe'ev, Dokl. Akad. Nauk. SSSR 52 (1946) 511.
[53] H. Liu, R.M. Sullivan, J.C. Hanson, C.P. Grey, J.D. Martin, J. Am. Chem. Soc. 123 (2001) 7564.
[54] J.D. Hancock, J.H. Sharp, J. Am. Ceram. Soc. 55 (2) (1972) 74.
[55] W.A. Johnson, R.F. Mehl, Trans. AIME 135 (8) (1939) 41.

[56] R.A. Gardner, J. Sol. Stat. Chem. 9 (1974) 336.
[57] H. Wang, W.J. Thomson, AIChE J. 41 (7) (1995) 1790.
[58] M. Shimokawabe, Thermochim. Acta 28 (1979) 287.
[59] M.V.C. Sastri, R.P. Viswanath, B. Viswanath, Int. J. Hydrogen Energy 7 (1982) 951.
[60] A.-H.A. El-Geassy, Scand. J. Metal. 27 (1998) 205.
[61] J. Moon, C.H. Rhee, Proceedings of the 1997 TMS Annual Meeting, Orlando, FL, Minerals Metals and Materials Society, Warrendale, PA, USA, 1997, p. 649.
[62] A.M. Ginstling, B.I. Brounshtein, Zh. Prikl. Khim. 23 (1950) 1327.
[63] B.B.L. Seth, H.U. Ross, Can. Metall. Quart. 5 (4) (1966) 315.
[64] W. Jander, Z. Anorg. AUg. Chem. 163 (1927) 1.